Optical-Resolution Photoacoustic Microscopy with Ultrafast Dual-Wavelength Excitation

Yingying Zhou[1,2,3], Siyi Liang[2,4], Mingsheng Li[2,4], Chengbo Liu[5], Puxiang Lai[1,3,*], and Lidai Wang[2,4,*]

[1] Department of Biomedical Engineering, Hong Kong Polytechnic University, Hong Kong

[2] Department of Biomedical Engineering, City University of Hong Kong, Hong Kong

[3] The Hong Kong Polytechnic University Shenzhen Research Institute, Shenzhen, China

[4] City University of Hong Kong Shenzhen Research Institute, Shenzhen, China

[5] Research Laboratory for Biomedical Optics and Molecular Imaging, Shenzhen Institutes of Advanced Technology, Chinese Academy of Sciences, Shenzhen, China

***Correspondence:** P.L. puxiang.lai@polyu.edu.hk, and L.W. lidawang@cityu.edu.hk

Abstract

Functional and molecular photoacoustic microscopy requires pulsed laser excitations at multiple wavelengths with enough pulse energy. The recent development of stimulated Raman scattering in optical fiber offers a low-cost laser source for multi-wavelength photoacoustic imaging. In this approach, long fibers temporally separate different wavelengths via optical delay. The long-time delay in fiber may limit the highest pulse energy, leading to poor image quality. Shorter optical fiber is more favorable to achieve high pulse energy for multi-wavelength photoacoustic imaging. Shorter fiber, on the other hand, would cause subsequent PA signals to partially overlap. To address this challenge, a frequency-domain method is developed to separate two photoacoustic signals that are partially overlapped in time, based on which an ultrafast dual-wavelength excitation technique is achieved. The signal separation

method is validated in numerical simulation and phantom experiments. We show that when two photoacoustic signals are partially overlapped with a 50-ns delay, they can be recovered with 98% accuracy. We apply this ultrafast dual-wavelength excitation technique to *in vivo* optical-resolution photoacoustic microscopy (OR-PAM). Results demonstrate that A-lines at two wavelengths can be successfully separated, and sO_2 values can be reliably computed from the separated data. This ultrafast dual-wavelength excitation enables functional OR-PAM with reduced misalignment among different wavelengths. In addition, this ultrafast dual-wavelength excitation technique allows that a fiber-based stimulated Raman scattering laser generates high pulse energy for photoacoustic imaging. More importantly, the short dual-wavelength excitation time potentially paves the way to the fast and multi-parameter photoacoustic imaging for microvascular dynamics.

Keywords: Signal separation, multi-wavelength, fast dual-wavelength excitation, functional photoacoustic imaging

1. Introduction

Optical-resolution photoacoustic microscopy (OR-PAM) is a non-invasive imaging technique that offers optical-absorption contrast at a subcellular resolution [1]. Using multiple excitation wavelengths, OR-PAM can quantify different types of molecules according to their unique absorption spectra [2, 3]. For example, with two or more wavelengths, OR-PAM can image hemoglobin concentration and blood oxygen saturation (sO_2) [4, 5]. *In vivo* functional OR-PAM often needs high imaging speed to acquire dynamic physiological information and mitigate motion artifacts. Fast functional OR-PAM requires a laser source having two or more wavelengths, high pulse repetition rate, fast multi-wavelength excitation, and sufficient pulse energy for good signal-to-noise ratio (SNR) [6-8].

Several pulsed laser techniques have been developed for fast dual-wavelength excitation in OR-PAM. One method is to sequentially trigger two pulsed lasers [9, 10]. Another method is to use

an electro-optical modulator (EOM) to switch among different wavelengths [11, 12]. The third method is to generate multiple wavelengths via stimulated Raman scattering (SRS) [13, 14] and delay them differently with long optical fibers [6]. These methods require delay time between different wavelengths not less than one A-line duration to separate the signals. However, in fast OR-PAM, if the delay time between different wavelengths is comparable with the pulse repetition time of one wavelength, different wavelengths may excite spots significantly misaligned. To minimize this misalignment, the delay time between different wavelengths needs to be much shorter than the single-wavelength pulse repetition time. Furthermore, in the SRS approach, a long delay fiber, as required by the long delay time between different wavelengths, may limit the highest pulse energy it can deliver, leading to weak photoacoustic signals [15, 16]. Therefore, a short multi-wavelength excitation time is preferred for reducing misalignment and improving sensitivity.

In this work, we present a novel frequency-domain approach to separate partially overlapped PA signals reliably. First, we simulate the separation algorithm. Then, we use the SRS and fiber delay to implement 50-ns dual-wavelength excitation. In phantom experiments, we can separate the partially overlapped PA signals with a good SNR (only reduces by 1.4%). *In vivo* sO_2 is imaged using ultrafast dual-wavelength excitation, whose results are as accurate as of the conventional OR-PAM method.

2. Methods

2.1 System setup

A schematic of ultrafast dual-wavelength excitation OR-PAM is shown in Figure 1. A pulsed laser (7-ns pulse width, VPFL-G-20, Spectra-Physics) emits 532-nm wavelength. The pulse repetition rate of the laser is 4 kHz in this study. The laser beam is split into two paths by a polarization beamsplitter (PBS, PBS051, Thorlabs Inc). A half-wave plate (HWP1, GCL-060633, Daheng Optics) is placed before the PBS to adjust the energy ratio of the two paths.

One path transmits in free space. The other path is coupled into a 10-m polarization-maintaining single-mode optical fiber (PMF, HB450-SC, Fibercore) to delay the pulse by 50-ns. The 10-m fiber can be used as an optical delay line. With increased pulse energy, the 10-m PMF can also generate 558-nm wavelength via the SRS effect. Because the polarization state of the pump laser affects the SRS efficiency, a half-wave plate (HWP2) is placed before the 10-m PMF to adjust the polarization state. In sO_2 imaging, a bandpass filter (central wavelength: 558 nm, bandwidth: 10 nm, FB560-10, Thorlabs Inc) is placed after the 10-m fiber to pass the 558-nm wavelength and reject others. The two paths are combined with a 50/50 beamsplitter (BS, BS010, Thorlabs Inc) and then delivered to an OR-PAM probe via a 2-m single-mode fiber (SM, P1-460B-FC-2, Thorlabs Inc). The fiber coupling efficiencies are above 50%.

In the OR-PAM probe, light from the 2-m fiber is focused by two achromatic doublets (AC064-013-A, Thorlabs Inc). An optical/acoustic beam combiner reflects the optical beam to the sample. At one laser trigger, the laser source excites two photoacoustic waves. Because of the 50-ns time delay, the two waves are partially overlapped. The photoacoustic waves are collimated by an acoustic lens (Stock #45-697, Edmund Optics), transmit through the optical/acoustic beam combiner, and are received by a piezoelectric transducer (V214-BC-RM, Olympus-NDT). Following one laser trigger, we acquire a one-dimensional depth-resolved signal, which consists of two partially overlapped PA signals. The data acquisition card (ATS9360, Alazar Tech Inc) digitizes the signal with 12-bit resolution at 500 MHz (The minimum sampling frequency required is 180 MHz). Raster scanning the PA probe allows for acquiring a volumetric image. Due to 50-ns time delay, the highest A-line rate can reach 10 MHz and the highest pulse repetition rate of the laser can reach 5 MHz, which can achieve ultrafast imaging speed. Because the ultrafast dual-wavelength excitation approach is not limited to a specific design of OR-PAM system, we use an OR-PAM system that has been published to demonstrate and validate our proposed method. The lateral resolution of this OR-PAM system is better than 5 μm. The axial resolution, determined by the bandwidth profile of

the ultrasonic transducer, is ~ 40 μm. Detailed information on the OR-PAM system can be found in [6, 17].

2.2 Principle

The dual-wavelength excitation time interval corresponding to the 10-m PMF is 50-ns. If the imaging depth range is 300 μm, an A-line may last for about 200-ns. In this case, the two PA signals are partially overlapped. In sO_2 imaging, the blood at 532 nm and 558 nm usually has similar small absorption coefficients. In addition, ranging from the nature of ballistic light, which OR-PAM adopts, the penetration depth is shallow, about 200 μm. Within this depth, we can assume that only one blood vessel dominates the PA signal. With the help of above-mentioned facts, it is reasonable to assume that the two PA signals have the same waveforms that the second PA signal is the delay copy (known time delay, which is decided by the delay-fiber length) of the first PA signal and multiplied by a value of k (the amplitude for two PA signals may be different due to laser fluence difference and some other effect). Their relationship can be expressed as

$$y_2(t) = k y_1(t - \Delta t), \quad (1)$$

where $y_1(t)$ and $y_2(t)$ are the first and second true PA signals, k is an unknown coefficient, and Δt is a known time delay between the two excitations. The detected PA signal y(t) is an overlap of the two A-lines, which can be written as

$$\mathrm{y(t)} = y_1(t) + k y_1(t - \Delta t) + e(t), \quad (2)$$

where e(t) is a random measurement noise.

To separate the two partially overlapped signals, we apply Fourier transform to Eq. (2) and obtain

$$\mathrm{Y}(\omega) = (1 + k\exp(-i\omega\Delta t))Y_1(\omega) + E(\omega). \quad (3)$$

We define $\hat{Y}_1(\omega) = \frac{Y(\omega)}{1+\hat{k}\exp(-i\omega\Delta t)}$, where $\hat{Y}_1(\omega)$ and $\hat{k}$ are estimated $Y_1(\omega)$ and k.

If $\hat{k} = k$, $\hat{Y}_1$ becomes

$$\hat{Y}_1(\omega) = Y_1(\omega) + \frac{E(\omega)}{1+\hat{k}\exp(-i\omega\Delta t)}. \quad (4)$$

Taking inverse Fourier transform of Eq. (4), we obtain

$$\hat{y}_1(t) = y_1(t) + e(t) \star m(t), \quad (5)$$

where the asterisk $\star$ denotes convolution operation, and $m(t)$ is the inverse Fourier transform of $[1 + \hat{k}\exp(-i\omega\Delta t)]^{-1}$.

Estimation of the A-line y_1 and k becomes an optimization problem

$$\min_{\hat{k}} \sum_{t=0}^{\infty} [\hat{y}_1(t) - y_1(t)]^2. \quad (6)$$

Because y_1 is directly measured before the second laser pulse excitation, i.e., $y(t) = y_1(t) + e(t)$ for $t < \Delta t$, we change the optimization problem to

$$\min_{\hat{k}} \sum_{t=0}^{\Delta t} [\hat{y}_1(t) - y(t)]^2. \quad (7)$$

Solving Eq. (7) allows us to separate the two signals and determine the amplitude ratio *k*.

3. Results and Discussion

3.1 Simulation

As shown in Figure 2, we simulate PA signal separation with different time delays. First, we acquire an A-line signal from a black tape sample with a single-pulsed excitation. To reduce noise, we average the signal by 1000 times. Then the A-line signal is multiplied by a constant coefficient *k* (varying from 0.74 to 1.32) and delayed by 10~60 ns. The original signal (blue solid line) and its delayed copy (red dashed line) are shown in Figure 2a. Random Gaussian white noise (standard deviation is 0.014) is added to the overlapped signal, resulting in an SNR of 25 dB. Figure 2b shows the overlapped signal. The Fourier-domain separation method is used to recover the original and delayed signals. The separation results are shown in Figure 2c. The correlation coefficients between the separated and true signals for the 1st and 2nd signals are 98.82% and 99.54%, respectively. The amplitude between the separated signals and true

signals are compared. A paired *t-test* gives p-values above 0.70, showing the separated signals are not significantly different from the true signals. We also compare the SNRs of the signals before and after separation. The average SNR is reduced by only 1.2% after the separation. P-value between the two groups is above 0.5, indicating the reduction is not significant.

We further test signal separation with different time delays from 10 to 60 ns. The SNR of the overlapped signal is 25dB. As shown in Figure 2d, when the time delay between two signals is not less than 18-ns (90% overlap), the separation correctness is greater than 97.42%.

3.2 Phantom

Phantom experiments are conducted to further validate the signal separation method. Figure 3a shows an overlapped PA signal generated from a black tape sample. SNR of the overlapped signal is 31 dB. The time delay between the two excitations is 50 ns. Using the proposed separation method, the first (blue solid line) and the second (red dashed line) PA signals are recovered and shown in Figure 3b. The separated amplitude of the second PA signal is 1.14 times of the first one (k=1.14). To verify the separation results, the first and second PA signals are directly measured with traditional single-pulse excitations. The measured signals are shown in Figure 3c. The correlation coefficients between the measured and separated PA signals are 0.979 for the first signal and 0.976 for the second signal. Compared with the direct measurement, the separated signals do not have significantly different peak-to-peak values (0.17%) and SNRs (1.4%). We further investigate the separation method at different SNRs. As shown in Figure 3d, the separation accuracy increases with the improved SNR. The correlation coefficients between the separated and the directly measured signals are higher than 94% when the SNR is above 23 dB. When the overlapped signal's SNR is greater than 30dB, the correlation coefficient is close to 100%. When the SNR of the overlapped signal is below 18 dB, the separated signals have low similarity (< 58%) with the directly measured signals.

Because the time delay between the two pulses is only sub-microseconds, the Grueneisen parameter may change due to instantaneous local heating [18]. We test the increase of the Grueneisen parameter in the dual-pulse excitation. The time delay between the two pulses is 50 ns. The pulse energies are both 50 nJ, which can excite PA signals with a high SNR (> 36dB). In the experiment, the second PA signal of a black tape sample is measured with and without the first pulse excitation. The second PA amplitude with the first pulse excitation is 0.8% (less than noise standard deviation 0.014) higher than the one without the first pulse excitation. Therefore, we can conclude that, with a reasonably high SNR, the Grueneisen parameter is not increased significantly in the dual-pulse excitation. When the first pulse energy is high, we need to further test if it will increase the Grueneisen parameter.

3.3 *In vivo*

We apply the Fourier-domain signal separation method to ultrafast dual-wavelength excitation in functional OR-PAM of the mouse ear. All procedures in the animal experiments were approved by the animal ethical committee of the City University of Hong Kong. Laser pulse repetition rate is 4 kHz. Two pulses at 532 nm and 558 nm are delayed by 50 ns. The pulse energy is 50 nJ for both wavelengths. In the raster scanning, the step size is 2.5 μm. The field of view is about 4.75×3.25 mm^2. The overlapped A-lines are acquired. We use the frequency-domain method to separate an overlapped PA signal to two signals and determine the amplitude ratio (*k* value) of them in each A-line. Then, maximum-amplitude projected (MAP) image corresponding to 532nm and 558nm are computed. Figure 4a and 4b shows separated square root of MAP images at 532 and 558 nm. Based on the separation MAP results of 532 nm and 558 nm, we determine the oxygen saturation using [19]

$$\boldsymbol{sO_2} = \frac{\boldsymbol{\varepsilon_{de}(\lambda_{558})PA(\lambda_{532})-\varepsilon_{de}(\lambda_{532})PA(\lambda_{558})}}{\boldsymbol{[\varepsilon_{ox}(\lambda_{532})-\varepsilon_{de}(\lambda_{532})]PA(\lambda_{558})-[\varepsilon_{ox}(\lambda_{558})-\varepsilon_{de}(\lambda_{558})]PA(\lambda_{532})}}, \quad (8)$$

where $\boldsymbol{\varepsilon_{ox}}$ and $\boldsymbol{\varepsilon_{de}}$ are the molar extinction coefficients of oxy- and deoxy-hemoglobin, and PA is the separated signal amplitude at different wavelengths. The sO_2 image is shown in Figure 4c. Figure 4d is another sO_2 image of the same region measured without using the signal separation, i.e., the 532-nm and 558-nm pulses are temporally separated by 200 ns and thus have no overlapping. It takes about six hours and less than 2 minutes to process and acquire Figure 4c and 4d, respectively. Figure 4e shows the averaged sO_2 values in three artery-vein pairs as labeled in Figure 4c and 4d. The SNR is above 18 dB. The difference between the sO_2 values obtained from the two methods is not significant, validating that the signal separation method can be applied to *in vivo* sO_2 imaging. The ultrafast dual-wavelength excitation enables the use of a short optical delay fiber and thus allows generating high pulse energy in stimulated Raman scattering laser.

4. Conclusion

We present a new ultrafast dual-wavelength excitation method for OR-PAM. Via stimulated Raman scattering and an optical fiber delay line, we can excite two PA signals at different optical wavelengths in tens of nanoseconds. The two PA signals may have significant overlapping. To address this issue, we develop a Fourier-domain signal separation method to recover the two PA signals. We assume that the two PA signals have the same waveform so that the amplitude ratio of the two signals can be determined via solving an optimization problem. We validate the method with numerical simulation and phantom experiments. Partially overlapped PA signals are separated with good accuracy. With a reasonably good SNR (only reduces by 1.4%), the separated two signals have the same peak-to-peak values with the true signals. Applying this method to *in vivo* OR-PAM, we demonstrate OR-PAM of oxygen saturation in the mouse ear. The results are comparable with the ones from conventional OR-PAM with long dual-wavelength excitation time. The ultrafast dual-wavelength excitation enables functional OR-PAM with reduced misalignment among different wavelengths. This

technique can potentially increase the pulse energy in SRS laser due to the short fiber length, which is beneficial to fast functional OR-PAM, such as single-red-blood-cell imaging, that requires high sensitivity and precise alignment among different wavelengths.

Acknowledgment

The work was supported in part by the National Natural Science Foundation of China (81671726, 81627805, and 81930048), the Hong Kong Research Grant Council (25204416, 21205016, 11215817, and 11101618), the Shenzhen Science and Technology Innovation Commission (JCYJ20170818104421564, JCYJ20160329150236426, and JCYJ20170413140519030), and the Hong Kong Innovation and Technology Commission (ITS/022/18).

Conflict of interest

L.W. has a financial interest in PATech Limited, which, however, did not support this work.

References

1. Wang, L.H.V. and S. Hu, *Photoacoustic Tomography: In Vivo Imaging from Organelles to Organs.* Science, 2012. **335**(6075): p. 1458-1462.
2. Yao, J.J. and L.H.V. Wang, *Photoacoustic microscopy.* Laser & Photonics Reviews, 2013. **7**(5): p. 758-778.
3. Beard, P., *Biomedical photoacoustic imaging.* Interface Focus, 2011. **1**(4): p. 602-631.
4. Zhang, H.F., et al., *Functional photoacoustic microscopy for high-resolution and noninvasive in vivo imaging.* Nature Biotechnology, 2006. **24**(7): p. 848-851.
5. Cao, F., et al., *Photoacoustic Imaging in Oxygen Detection.* Applied Sciences-Basel, 2017. **7**(12).
6. Liang, Y.Z., et al., *2 MHz multi-wavelength pulsed laser for functional photoacoustic microscopy.* Optics Letters, 2017. **42**(7): p. 1452-1455.
7. Shi, W., et al., *In vivo near-realtime volumetric optical-resolution photoacoustic microscopy using a high-repetition-rate nanosecond fiber-laser.* Optics Express, 2011. **19**(18): p. 17143-17150.
8. Yamaoka, Y., et al., *Photoacoustic microscopy using ultrashort pulses with two different pulse durations.* Optics Express, 2014. **22**(14): p. 17063-17072.
9. Ning, B., et al., *Simultaneous photoacoustic microscopy of microvascular anatomy, oxygen saturation, and blood flow.* Optics Letters, 2015. **40**(6): p. 910-913.

10. Wang, Y., et al., *In vivo integrated photoacoustic and confocal microscopy of hemoglobin oxygen saturation and oxygen partial pressure.* Optics Letters, 2011. **36**(7): p. 1029-1031.
11. Hu, S., et al., *Dichroism Optical-resolution Photoacoustic Microscopy.* Photons Plus Ultrasound: Imaging and Sensing 2012, 2012. **8223**.
12. Wang, T., et al., *Multiparametric photoacoustic microscopy of the mouse brain with 300-kHz A-line rate.* Neurophotonics, 2016. **3**(4): p. 045006.
13. Hajireza, P., A. Forbrich, and R. Zemp, *In-Vivo functional optical-resolution photoacoustic microscopy with stimulated Raman scattering fiber-laser source.* Biomed Opt Express, 2014. **5**(2): p. 539-46.
14. Koeplinger, D., M.Y. Liu, and T. Buma, *Photoacoustic microscopy with a pulsed multi-color source based on stimulated Raman scattering.* 2011 Ieee International Ultrasonics Symposium (Ius), 2011: p. 296-299.
15. Stolen, R.H., et al., *Raman Response Function of Silica-Core Fibers.* Journal of the Optical Society of America B-Optical Physics, 1989. **6**(6): p. 1159-1166.
16. Andersen, J.F., J. Busck, and H. Heiselberg, *Pulsed Raman fiber laser and multispectral imaging in three dimensions.* Applied Optics, 2006. **45**(24): p. 6198-6204.
17. Wang, L.D., et al., *Fast voice-coil scanning optical-resolution photoacoustic microscopy.* Optics Letters, 2011. **36**(2): p. 139-141.
18. Lai, P.X., et al., *Photoacoustically guided wavefront shaping for enhanced optical focusing in scattering media.* Nature Photonics, 2015. **9**(2): p. 126-132.
19. Zhang, H.F., et al., *Imaging of hemoglobin oxygen saturation variations in single vessels in vivo using photoacoustic microscopy.* Applied Physics Letters, 2007. **90**(5).

Figures

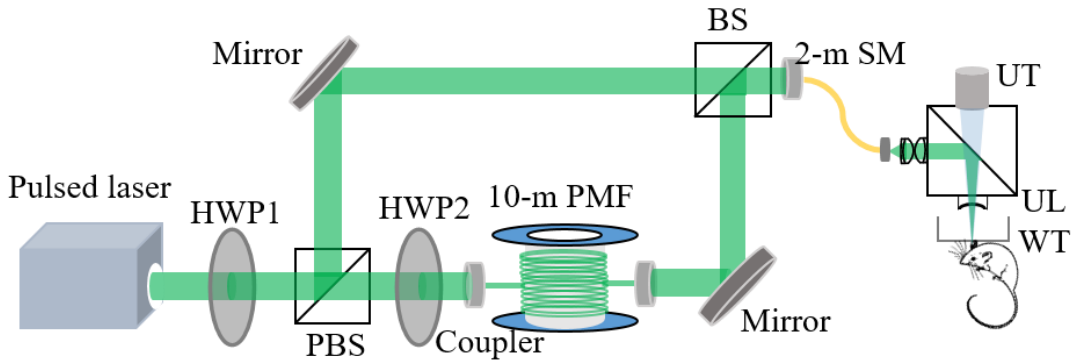

Figure 1. Schematic of OR-PAM with ultrafast dual-wavelength excitation. BS, beamsplitter; HWP, halfwave plate; PBS, polarizing beamsplitter; PMF, polarization-maintaining fiber; SMF, single-mode fiber; UL, ultrasound lens; UT, ultrasound transducer; WT, water tank.

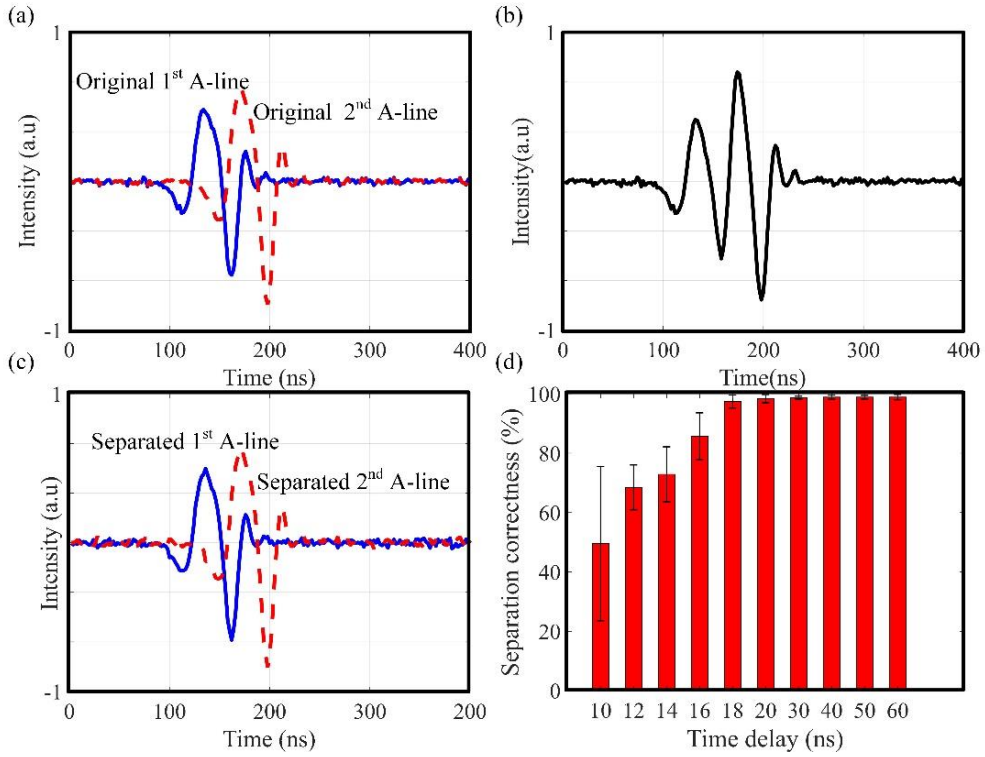

Figure 2. Numerical simulation of signal separation. (a) An acquired A-line excited with one pulse (blue solid line) and its delayed copy (red dashed line). The copy is delayed by 50-ns and multiplied by k. (b) Summation of the two signals to simulate ultrafast dual-pulse excitation. (c) The separated first signal (blue solid line) and the separated second signal (red dashed line).

(d) Separation correctness versus delay time. The separation correctness is defined as $|\hat{k} - k|/k$. *Error bars are standard deviation, and the sample size is 20.*

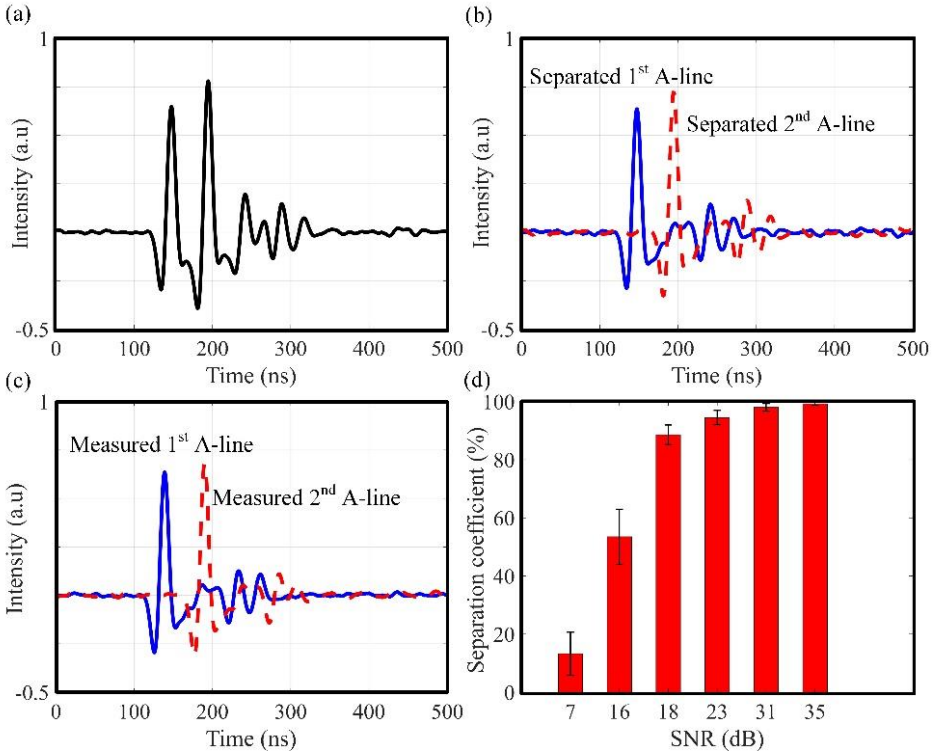

Figure 3. Phantom experiments of signal separation on black-tape samples. (a) Dual-pulse overlapped PA signal. (b) Separated PA signals. (c) Directly measured PA signals. (d) The correlation coefficients between the separated and directly measured signals at different SNRs. Error bars are standard deviations, and the sample size is 20.

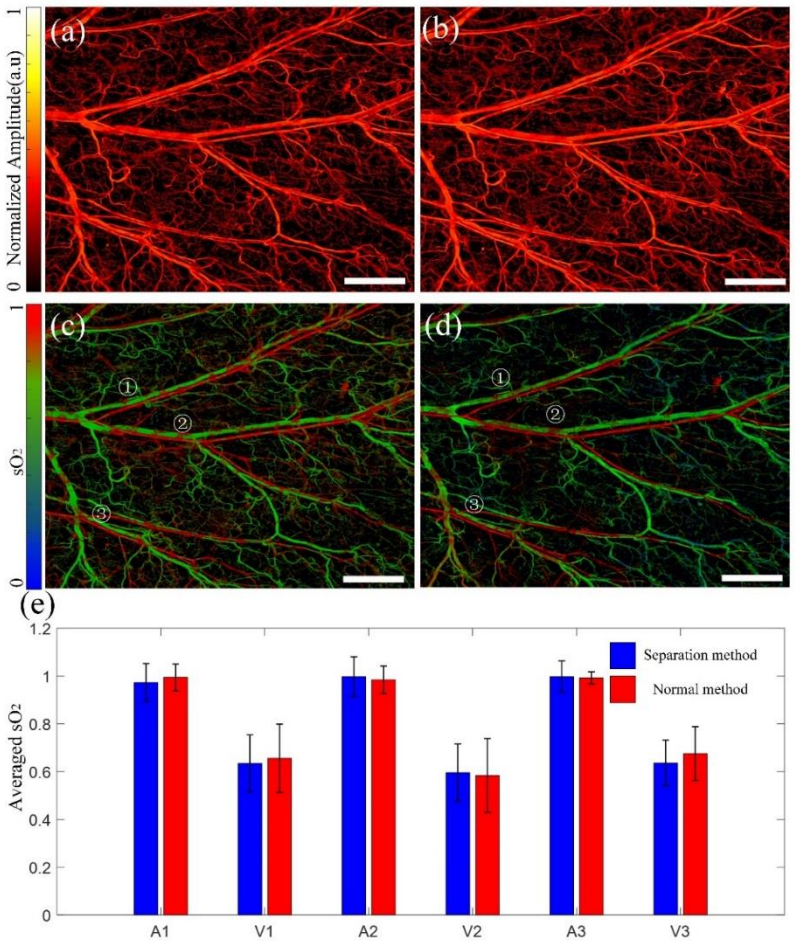

Figure 4. In vivo OR-PAM of oxygen saturation with ultrafast dual-wavelength excitation. The first and second pulses are 532 nm and 558 nm. The time delay is 50 ns. (a) Separated first PA image (532-nm) of the mouse ear. (b) Separated second PA image (558-nm) of the mouse ear. (c) Oxygen saturation image of the mouse ear calculated from the separated data. (d) Oxygen saturation image of the same mouse ear calculated from two single-pulse excitation data at 532 and 558 nm. The two pulses are delayed by 200 ns and thus have no overlapping. (e) Comparison of sO_2 values in three artery-vein pairs measured with the two methods. The artery-vein pairs are labeled in (c) and (d). Scale bar: 800 μm.